Title
Optimized doppler optical coherence tomography for choroidal capillary vasculature imaging

ISBN
9780819484260

Authors
Liu, Gangjun
Qi, Wenjuan
Yu, Lingfeng
et al.

Publication Date
2011-02-10

DOI
10.1117/12.876066

Optimized Doppler optical coherence tomography for choroidal capillary vasculature imaging

Gangjun Liu[1,2], Wenjuan Qi[1], Lingfeng Yu[1], Zhongping Chen[1,2]
1. Beckman Laser Institute, University of California, Irvine, Irvine, CA, 92612
2. Department of Biomedical Engineering, University of California, Irvine, Irvine, CA, 92617

ABSTRACT

In this paper, we analyzed the retinal and choroidal blood vasculature in the posterior segment of the human eye with optimized color Doppler and Doppler variance optical coherence tomography. Depth-resolved structure , color Doppler and Doppler variance images were compared. Blood vessels down to capillary level were able to be obtained with the optimized optical coherence color Doppler and Doppler variance method. For in-vivo imaging of human eyes, bulk-motion induced bulk phase must be identified and removed before using color Doppler method. It was found that the Doppler variance method is not sensitive to bulk motion and the method can be used without removing the bulk phase. A novel, simple and fast segmentation algorithm to indentify retinal pigment epithelium (RPE) was proposed and used to segment the retinal and choroidal layer. The algorithm was based on the detected OCT signal intensity difference between different layers. A spectrometer-based Fourier domain OCT system with a central wavelength of 890 nm and bandwidth of 150nm was used in this study. The 3-dimensional imaging volume contained 120 sequential two dimensional images with 2048 A-lines per image. The total imaging time was 12 seconds and the imaging area was 5x5 mm^2.

Keywords: optical coherence tomography, laser Doppler.

1. Introduction

Optical coherence tomography (OCT) is a powerful interferometric technology that is used to obtain tissue cross section images noninvasively with micrometer resolution, millimeter penetration depth and video-rate imaging speed [1]. OCT has become a valuable tool in a number of medical fields, especially in ophthalmology due to its non-contact, high resolution nature. Extension of the OCT technique to functionally image the human eye is of great interest. Doppler optical coherence tomography (DOCT) is one kind of functional extension of OCT which combines the Doppler principle with OCT and provides in-vivo imaging of blood vessels, blood flow direction, and flow speed [2-14].

Blood flow in humans is complex. The flow is pulsatile. The flow speed in a blood vessel is not a constant value, and it changes from the center to the edge in the blood vessel. A parabolic equation may usually describe the distribution of the steady blood flow along the blood vessel radius. This kind of steady flow is usually called laminar flow. The laminar flow may breakdown into a turbulent flow when its velocity is high [15]. In practice, the Doppler frequency produced by a single target will produce a spectrum of Doppler frequency or a series of frequency shift instead of a single frequency. This spectrum broadening is attributed to several sources, such as the cone-geometrical focusing beam, Brownian motion and the speckle. Brownian motion dominates the broadening of the Doppler spectrum at low flow speed, and probe-beam geometry dominates at high flow speed [16]. Depending on the Doppler frequency shift information obtained, we can display this information in a color Doppler method or a variance method. In the color Doppler imaging method, the average Doppler frequency shift is displayed as color images, and the negative and positive averaged frequency shifts are displayed in different colors [2-4]. In color Doppler images, the information regarding the flow speed and flow direction can be obtained. In a Doppler variance image, the variance or the standard deviation of the Doppler frequency shift is displayed [5].

In early time domain OCT systems, the Doppler frequency shift was obtained by a spectrogram method which used the short time fast Fourier transformation (STFFT) or wavelet transformation [2-4]. However, the spectrogram method allowed detection of high speed flow only, and a phase-resolved method was introduced to solve this problem [6]. Phase-resolved Color Doppler has been successfully used to analyze retinal blood flow in real-time [7, 8]. While it was thought that it is hard for phase-resolved OCT method to get the blood vessel networks in the choroid [9], several methods have

Optical Coherence Tomography and Coherence Domain Optical Methods in Biomedicine XV, edited by James G. Fujimoto, Joseph A. Izatt, Valery V. Tuchin, Proc. of SPIE Vol. 7889, 78890J · © 2011 SPIE · CCC code: 1605-7422/11/$18
doi: 10.1117/12.876066

been introduced by different group to overcome this problem [9-12]. Wang et al. proposed a method called optical microangiography (OMAG) technology to separate the static and moving signals with a modified Hilbert transform [9,11]. By stitching multiple small scanning areas, high-resolution choroid blood vessel images down to the capillary level were demonstrated with OMAG technology [9, 10]. However, the introducing of the Hilbert transform increases the algorithm complexity and computing time. Imaging multiple small areas will increase the imaging time, and registering several small area images into one image is technically challenging. Another method named Joint Spectral and Time Domain OCT also demonstrated the detection of capillary level blood vessels [12, 13]. However, this method needed high scanning density and may increase imaging time greatly. Recently, our group has demonstrated imaging of retinal and choroid blood using phase-resolved Doppler variance imaging [14].

In this paper, we show that imaging choroidal capillary vasculature network is possible with phased-resolved color Doppler and Doppler standard deviation without sacrificing the imaging time and data processing time. For in-vivo applications, especially ophthalmology, axial sample movement will induce bulk motion and change the detected Doppler frequency. The axial sample movement induced artifacts must be corrected before applying the optical Doppler tomography algorithm. Histogram-based methods are often used to get the bulk motion induced bulk phase. However, this method may also introduce artifacts. We show that Doppler variance was insensitive to bulk motion of the imaged sample and may be used without removal of bulk motion. A novel, simple and fast segmentation algorithm to indentify retinal pigment epithelium (RPE) is proposed and used to segment the retinal and choroidal layer. High resolution imaging of choroidal capillary vasculature network with phased-resolved color Doppler and Doppler variance is demonstrated.

2. Method

Phase-resolved Doppler OCT has dominated the methods to extract the average Doppler frequency, and it is based on the detection of the phase difference between adjacent A-lines [6, 17].

$$\overline{f} = \frac{\int fP(f)df}{\int P(f)df} = \frac{d\theta(z)}{dt} = \frac{\theta_{j+1,z} - \theta_{j,z}}{T} \qquad (1)$$

where $\overline{f}$ is Doppler frequency and $P(f)$ is the power spectrum of the Doppler frequency shift, $\theta_{j+1,z}$ and $\theta_{j,z}$ are phase for the signal at depth z of $(j+1)th$ and jth A-line. As we know,

$$\begin{aligned}\tan(\theta_{j+1,z} - \theta_{j,z}) &= \frac{\tan(\theta_{j+1,z}) - \tan(\theta_{j,z})}{1 + \tan(\theta_{j+1,z})\tan(\theta_{j,z})} \\ &= \frac{\dfrac{\mathrm{Im}(A_{j+1,z})}{\mathrm{Re}(A_{j+1,z})} - \dfrac{\mathrm{Im}(A_{j,z})}{\mathrm{Re}(A_{j,z})}}{1 + \dfrac{\mathrm{Im}(A_{j+1,z})\,\mathrm{Im}(A_{j,z})}{\mathrm{Re}(A_{j+1,z})\,\mathrm{Re}(A_{j,z})}} \\ &= \frac{\mathrm{Im}(A_{j+1,z})\,\mathrm{Re}(A_{j,z}) - \mathrm{Im}(A_{j,z})\,\mathrm{Re}(A_{j+1,z})}{\mathrm{Re}(A_{j,z})\,\mathrm{Re}(A_{j+1,z}) + \mathrm{Im}\,A_{j+1,z})\,\mathrm{Im}(A_{j,z})} \qquad (2)\end{aligned}$$

where, $\mathrm{Re}(A_{j,z})$ and $\mathrm{Im}(A_{j,z})$ are the real and imaginary parts of the complex data $A_{j,z}$. So Eq.(1) can be rewritten as

$$\overline{f} = \arctan\left[\frac{\mathrm{Im}(A_{j+1,z})\,\mathrm{Re}(A_{j,z}) - \mathrm{Im}(A_{j,z})\,\mathrm{Re}(A_{j+1,z})}{\mathrm{Re}(A_{j,z})\,\mathrm{Re}(A_{j+1,z}) + \mathrm{Im}(A_{j+1,z})\,\mathrm{Im}(A_{j,z})}\right] \Big/ T. \qquad (3)$$

Equation 3 can also be derived from autocorrelation technology [17]. It is the so-called autocorrelation algorithm and has shown great success in the fields of both ultrasound Doppler imaging [17] and Doppler OCT [6].

Doppler variance is an extension of OCT/ODT technique. It uses the variance of the Doppler frequency spectrum to map the flow. Doppler variance has benefits of being less sensitive to the pulsatile nature of the blood flow, of being less

sensitive to the incident angle and may be used to obtain the transverse flow velocity [5, 14, and 16]. If σ denotes the standard deviation of the Doppler spectrum, the Doppler variance σ^2 can be obtained [5, 17]:

$$\sigma^2 = \frac{\int (f-\overline{f})^2 P(f) df}{\int P(f) df} = \overline{f^2} - \overline{f}^2 \quad . \tag{4}$$

With the help of autocorrelation technology, the variance can be expressed as [17]:

$$\sigma^2 = \frac{1}{T^2}\left(1 - \frac{\left|A_{j,z} A^*_{j+1,z}\right|}{A_{j,z} A^*_{j,z}}\right). \tag{5}$$

Usually, the equations are used together with averaging to improve signal noise ratio (SNR). Average could be done in the lateral direction (temporal direction) so that the equations (3) and (5) become [5, 6, and 17].

$$\overline{f} = \arctan\left\{\frac{\sum_{j=1}^{J}\left[\mathrm{Im}(A_{j+1,z})\,\mathrm{Re}(A_{j,z}) - \mathrm{Im}(A_{j,z})\,\mathrm{Re}(A_{j+1,z})\right]}{\sum_{j=1}^{J}\left[\mathrm{Re}(A_{j,z})\,\mathrm{Re}(A_{j+1,z}) + \mathrm{Im}(A_{j+1,z})\,\mathrm{Im}(A_{j,z})\right]}\right\} \Big/ T \,. \tag{6}$$

$$\sigma^2 = \frac{1}{T^2}\left[1 - \frac{\left|\sum_{j=1}^{J}\left(A_{j,z} A^*_{j+1,z}\right)\right|}{\sum_{j=1}^{J}\left(A_{j,z} A^*_{j,z}\right)}\right] \quad . \tag{7}$$

where J is the number of A-lines that are averaged. Averaging could also be performed in both lateral and depth direction and the equations (6) and (7) become [18, 19, 20],

$$\overline{f} = \arctan\left\{\frac{\sum_{j=1}^{J}\sum_{z=1}^{N}\left[\mathrm{Im}(A_{j+1,z})\,\mathrm{Re}(A_{j,z}) - \mathrm{Im}(A_{j,z})\,\mathrm{Re}(A_{j+1,z})\right]}{\sum_{j=1}^{J}\sum_{z=1}^{N}\left[\mathrm{Re}(A_{j,z})\,\mathrm{Re}(A_{j+1,z}) + \mathrm{Im}(A_{j+1,z})\,\mathrm{Im}(A_{j,z})\right]}\right\} \Big/ T \,. \tag{8}$$

$$\sigma^2 = \frac{1}{T^2}\left[1 - \frac{\left|\sum_{j=1}^{J}\sum_{z=1}^{N}\left(A_{j,z} A^*_{j+1,z}\right)\right|}{\sum_{j=1}^{J}\sum_{z=1}^{N}\left(A_{j,z} A^*_{j,z}\right)}\right]. \tag{9}$$

where J is the number of A-lines that are averaged and N is the number of depth points that are averaged. The chosen of J and N are dependent on application. Generally, a larger J and N will increase SNR, increase the computing time and decrease resolution. In this manuscript, we are using $J = 4$ for lateral averaging only images and $J = 4$, $N = 4$ for lateral and depth averaging images to balance the SNR and resolution.

Detail of the system used in this study can be found in references [14, 21]. Briefly, the spectrometer-based Fourier domain OCT using a SLD light source has a central wavelength of 890 nm and FWHM bandwidth of 150 nm. A modified scanning head from a commercial Zeiss Stratus OCT was used. The optical power on the human eye was set at 700 μW. The CCD integration time was set at 50 μs. The system sensitivity was measured to be about 100 dB at around zero imaging depth. A 6-dB sensitivity roll-off distance was found to be 1.6 mm imaging depth. Imaging process includes background signal subtraction, linear interpolation to convert data in linear wavelength space to linear wavenumber space, and numerical dispersion. The axial resolution was measured to be 3.5 μm.

3. Bulk motion insensitive Doppler variance imaging

For in vivo application of Doppler OCT, the axial sample movement will induce bulk motion and change the detected Doppler frequency. In order to accurately get the Doppler frequency induced by the blood vessel only, the sample-induced bulk motion must be removed. For the phased-resolved Doppler method, the most common method to remove bulk motion is to find the bulk motion induced bulk phase. Up to now, several methods have been proposed to extract the bulk phase and most of the methods are based on the histogram-based method [19]. Usually, the histogram-based method estimates the median phase, or mean phase and then subtracted it. Recently, averaged-shift-histogram-based nonparametric density estimators have become popular to extract the bulk phase [22, 23]. These histogram-based methods show success in different situations, however, these method increase the computation complexity and time. In this paper, we show that the Doppler variance method does not suffer from bulk motion-induced artifacts and can be used to extract the capillary blood vessel network in human choroid without the bulk phase removal.

Figure 1 (a) shows the OCT images of human retinal region. The images shown have a scanning range of 5 mm and including 2048 A-lines. Figs.1 (b) and (c) show lateral averaging color Doppler and Doppler variance OCT images without bulk motion correction; Figs.1 (d) and (e) show lateral averaging color Doppler and Doppler variance OCT images with bulk motion correction; Figs. 1(f) and (g) show lateral and depth averaging color Doppler and Doppler variance images without bulk phase removal. Figs. 1(h) and (i) show lateral and depth averaging color Doppler and Doppler variance images with bulk phase removal. The bulk phase was removed by the histogram method introduced in reference 14. From these figures, we found that color Doppler is affected by the bulk motion more than Doppler variance is. The bulk motion increases the background signal of the color Doppler image and blood vessels cannot be indentified if the bulk motion is very strong as shown in the region inside the red circle in Fig.1(b) and Fig.1(f). Bulk motion induced motion artifacts must be corrected before applying color Doppler algorithm. The bulk motion corrected images as demonstrated in Fig.1 (d) and Fig.1 (f) show great improvement. By comparing Fig.1(d) with Fig.1(f), it can be found that, with the lateral and depth averaging, the signal to noise ratio is also improved. As for the lateral averaging Doppler variance images [Figs. 1 (c) and (e)], there is background signal. This could be found by comparing Fig. 1 (c) with Fig. 1(e). However, the blood vessels in the high bulk motion region can still be identified even without correction of the bulk motion as shown in the red circle in Fig.1 (c). The lateral and depth averaging Doppler variance images [Fig. 1(g) and Fig.1(i)] show insensitivity to the bulk-motion effects. The Doppler variance images [Fig.1(g)] without bulk motion correction show great similarity to the bulk motion corrected Doppler variance images [Fig.1(i)].

In the region with large blood vessels, histogram based bulk motion correction may introduce artifacts as indicated by the red arrows in Figs. 1 (b), Fig.1(c), Fig.1(h) and Fgi.1(i). These artifacts may be corrected with the improved phase-resolved algorithm proposed in reference 21. Although effective, the improved algorithm in reference 21 may increase the calculation time and complexity. As demonstrated in this manuscript, the lateral and depth averaging Doppler variance images are not sensitive to bulk motion and may be used without the bulk motion correction. The Doppler variance images without bulk motion correction do not show the artifacts.

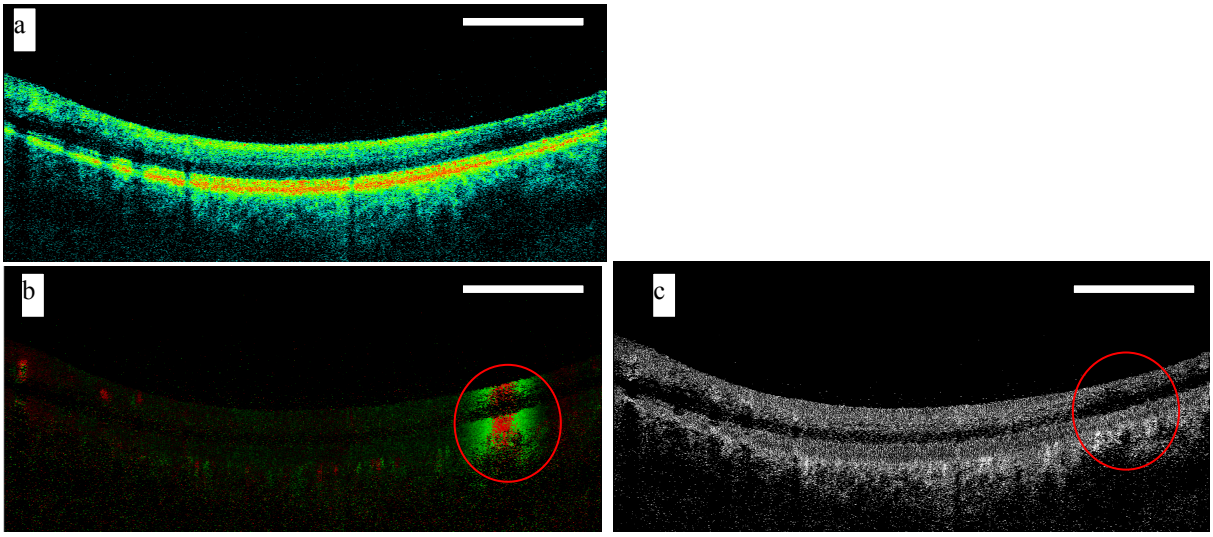

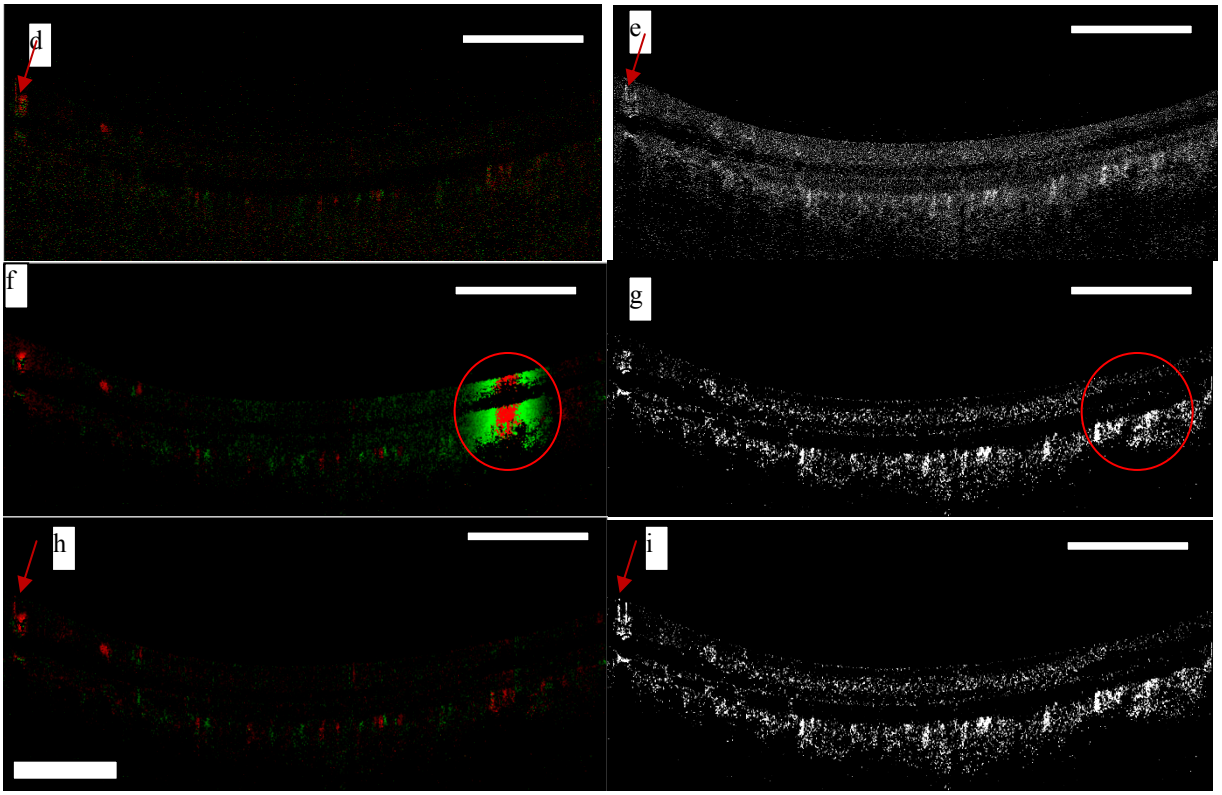

Fig. 1(a) OCT intensity image; (b) lateral averaging color Doppler OCT image without bulk motion correction; (c) lateral averaging Doppler variance OCT image without bulk motion correction; (d) lateral averaging color Doppler OCT image with bulk motion correction; (e) lateral averaging Doppler variance OCT image with bulk motion correction; (f) lateral and depth averaging Color Doppler OCT image without bulk motion correction; (g) lateral and depth averaging Doppler variance OCT image without bulk motion correction; (h) lateral and depth averaging color Doppler OCT image with bulk motion correction; (i) lateral and depth averaging Doppler variance OCT image with bulk motion correction. Scale bar: 1mm.

4. RPE layer identification

Depth-resolved information was needed to identify and segment different layers. In this paper, we were interested in the blood vessels in the choroidal layer. We will introduce a new method to do the retinal and choroid layer segmentation. When performing automatic segmentation of OCT images, the images usually need to be preprocessed with special filter to remove the speckles. Several filters, such as a mean filter [24] and a nonlinear complex diffusion filter [25], have been used to remove the speckles. In this paper, lateral and vertical averaging has been used to process ODT and variance images. This averaging technique was also used to process the OCT intensity images. Figs.2 (a) and (b) show the OCT images without and with the lateral and vertical averaging technique. We found the speckle noise was greatly reduced after processing the OCT intensity image with lateral and vertical averaging. This method is different from the medial filter used in the imaging process. The averaging was performed after the Fourier transform and before the logarithm calculation.

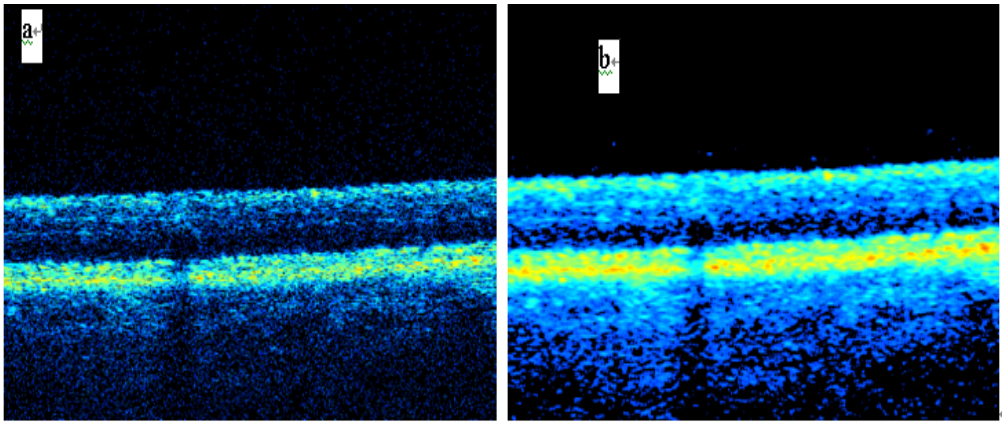

Fig.2 OCT images without (a) and with(b) lateral and vertical (depth) averaging.

The RPE layer has the strongest reflection, and it is commonly located by searching for the maximum reflection intensity[26]. However, there may be sporadic strong reflection from other layers, and blood vessels in the retinal layer may cause a "shadow" effect. These effects will affect the results of locating the RPE layer by the maximum intensity searching method. The layers in the retinal or choroid layers are usually smooth and continuous. The effects mentioned above cause discontinuity and a sharp change of the detected layer surface. A "top-hat" filtering was used from reference 26 to correct this. Here, we propose a simple method called "discontinuity filtering" (DF) method to solve this. After finding the maximum intensity location of each A-line, we can obtain an array. Usually, the central part of the array is more accurate. Starting from the middle cell of this array, we search for discontinuity in two directions. If the pixel difference between adjacent cells of the array is more than 40 pixels, we will think discontinuity is found and the value is not correct. The incorrect value is abandoned and filled with the value of the adjacent cell close to the center of the array. After the DF filter, a simple moving average (MA) method is used to make the curve smoother. Finally, a 6th order polynomial fitting is applied to get the final detected RPE layer. The different steps for this processing procedure are shown in fig. 3. In Fig. 4, the detected RPE layers with the proposed method are shown. In Figs. 4 (a), (b) and (c), the maximum intensity location is shown on the images. In Fig. 4(a), the arrows indicate the wrong RPE location detected due to the shadow effect and sporadic strong reflection from the retinal layer. In Figs. 4(d), (e) and (f), the proposed method detected RPE layers are shown. From the pictures in Fig. 4, we find that the current method is very efficient for the detection of the RPE layer even for special cases as shown in Fig. 4(c).

The algorithm for the layer segmentation was implemented in Microsoft Visual C++ 2008. The software runs on a Dell Vostro 200 desktop computer with a central processing unit **(**CPU) of Intel Core 2 Duo E7300 @ 2.66GHz. The software is designed with graphic user interface (GUI) for the user to choose the parameters, such as the moving average period, polynomial fitting order. For a moving average period of 8 and a fitting order of 6, the processing time to find the RPE layer of one OCT image with a size of 2048 $\times$700 pixels will be 0.054 seconds. Fabritius et al. compared the processing time of existing segmentation algorithms and proposed a faster algorithm which takes around 0.15s to obtain the RPE layer for one image with 1024 $\times$ 320 pixels[26]. The algorithm proposed here is much faster than the algorithm proposed by Fabritius et al. The proposed algorithm here may also be used to identify other layers, such as the internal limiting membrane (ILM) layer, as demonstrated in Fig. 5. The ILM layer may be identified by a pixel intensity threshold instead of the maximum intensity as for the case of RPE layer indentification. The threshold may be chosen manually by the operator. However, when processing more curvature layers, a higher order polynomial fitting may be used instead of the 6^{th} order.

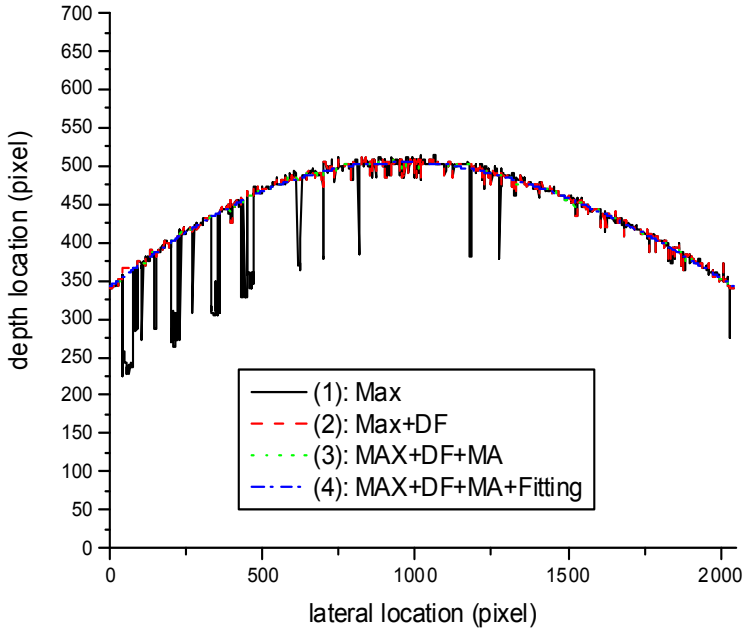

Fig. 3 The 4 steps to identify the RPE layer. (1) Max: Identifying the maximum intensity location; (2) Max+DF: "discontinuity filtering" applied to the first step. (3) Max+DF+MA: Moving average applied to the second step. (4). Max+DF+MA+Fitting: 6th order polynomial fitting applied to the third step. Scale bar: 1mm.

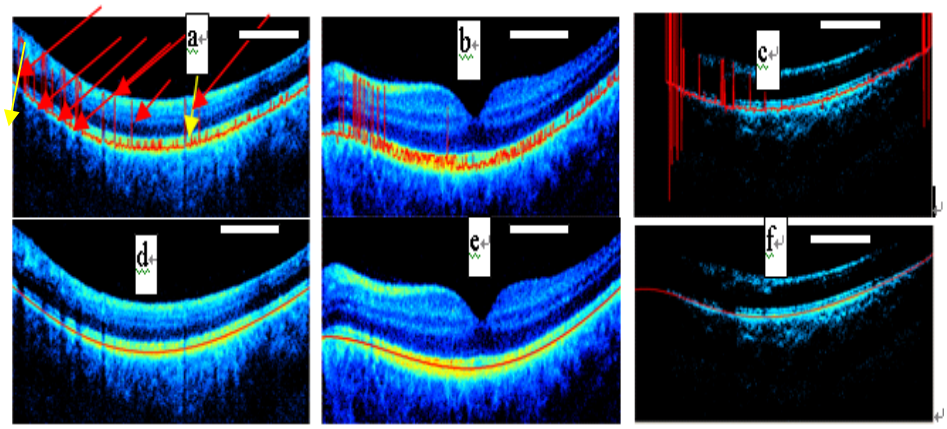

Fig. 4. (a), (b) and (c), the maximum intensity locations detected are shown on different OCT images. (d), (e) and (f), the proposed method detected RPE layers are shown on the images.

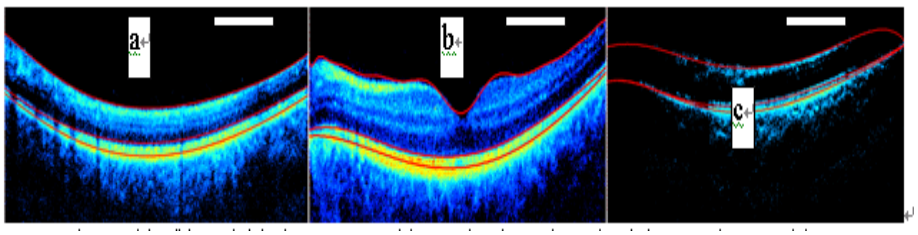

Fig. 5. (a), (b) and (c) the proposed intensity-based method detected several layers are overlayed on the images.

5. Results

The RPE layers were identified based on the OCT images. The detected RPE layer location was applied to the Doppler variance images and color Doppler images. The Doppler variance images were processed without the bulk motion removal. The color Doppler images were processed with bulk motion removal. The layers below the RPE layers were taken as choroidal layers. The projection OCT structure, Doppler variance and color Doppler images were obtained by summing up all the layers below the RPE layers. The results are shown in Fig. (5). Different blood vessels can be seen from these images. OCT images are based on the magnitude of backscattered or back-reflected light. Blood vessels usually manifest as low magnitude in OCT projection images. However, only large diameter blood vessels that are high absorptive can been seen from OCT projection images. Color Doppler projection images [Fig.5 (c)] can provide much more information about the blood vessel, such as blood flow direction (pink and blue colors represent different direction), blood flow speed etc. However, due to the pulsate nature of human blood flow, the blood flow direction and blood flow speed are not constant inside one blood vessel. The incident angle dependent nature of Doppler OCT makes the situation more complex. The information provided by color Doppler OCT are compromised. Doppler variance projection image provides a fine microvascular network image which is much clearer. Because Doppler variance projection images are obtained without bulk motion removal, the processing time is less and the processing procedure is much easier.

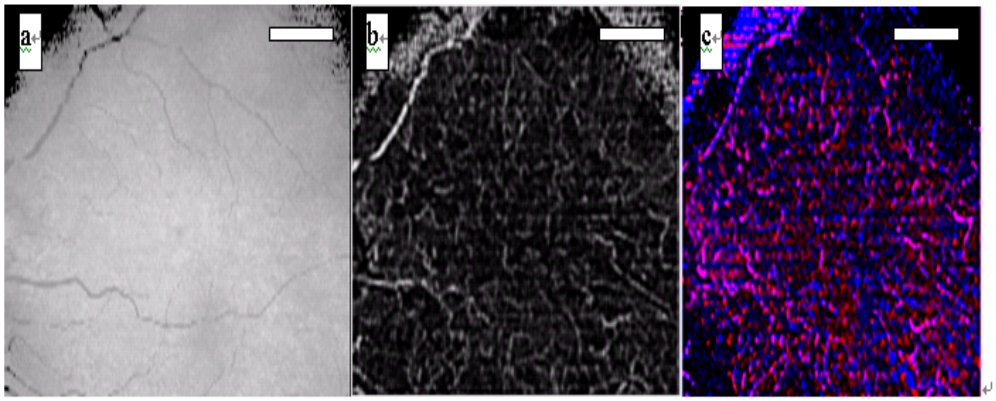

Fig. 5. (a) OCT, (b) Doppler variance and (c)color Doppler projection images of choroidal vessels.

Scale bar: 1mm.

6. Conclusions

We demonstrate a high resolution imaging of a choroidal capillary vasculature network with phased-resolved color Doppler and Doppler variance. The effect of temporal and depth averaging on the effect of color Doppler and Doppler variance images were analyzed. It was found that the temporal and depth averaging Doppler variance method is not sensitive to bulk motion, and the method can be used without removing the bulk phase. A novel, simple and fast segmentation algorithm to indentify retinal pigment epithelium (RPE) was proposed to segment the retinal and choroidal layer.

7. Acknowledgement

This work was supported by the National Institutes of Health (EB-00293, NCI-91717, RR-01192), Air Force Office of Scientific Research (FA9550-04-0101), and the Beckman Laser Institute Endowment.

References:

[1]. D. Huang, E. A. Swanson, C. P. Lin, J. S. Schuman, W. G. Stinson, W. Chang, M. R. Hee, T. Flotte, K. Gregory, C. A. Puliafito, and J. G. Fujimoto, "Optical coherence tomography," *Science* 254, 1178–1181 (1991).

[2]. Z. Chen, T. E. Milner, D. Dave, and J. S. Nelson, "Optical Doppler tomographic imaging of fluid flow velocity in highly scattering media," *Opt. Lett.* 22, 64–66 (1997).

[3]. Z. Chen, T. E. Milner, S. Srinivas, X. J. Wang, A. Malekafzali, M. J. C. van Gemert, and J. S. Nelson, "Noninvasive imaging of *in vivo* blood flow velocity using optical Doppler tomography," *Opt. Lett.* 22, 1119–1121 (1997).
[4]. J. A. Izatt, "*In vivo* bidirectional color Doppler flow imaging of picoliter blood volumes using optical coherence tomography," *Opt. Lett.* 22, 1439–1441 (1997).
[5]. Y. Zhao, Z. Chen, C. Saxer, S. Xiang, J. de Boer, and J. Nelson, "Doppler variance imaging for clinical monitoring of *in vivo* human skin blood flow," *Opt. Lett.* 25, 1358–1360 (2000).
[6]. Y. Zhao, Z. Chen, C. Saxer, S. Xiang, J. de Boer, and J. Nelson, "Phase resolved optical coherence tomography and optical Doppler tomography for imaging blood flow in human skin with fast scanning speed and high velocity sensitivity," *Opt. Lett.* 25, 114–116 (2000).
[7]. B. R. White, M. C. Pierce, N. Nassif, B. Cense, B. Park, G. Tearney, B. Bouma, T. Chen, and J. de Boer, "*In vivo* dynamic human retinal blood flow imaging using ultra-high-speed spectral domain optical Doppler tomography," *Opt Express*. 11, 3490–3497 (2003).
[8]. R. A. Leitgeb, L. Schmetterer, W. Drexler, A. F. Fercher, R. J. Zawadzki, and T. Bajraszewski, "Real-time assessment of retinal blood flow with ultrafast acquisition by color Doppler Fourier domain optical coherence tomography," *Opt Express*. 11, 3116–3121 (2003).
[9]. An L, Subhush HM, Wilson DJ, Wang RK., "High-resolution wide-field imaging of retinal and choroidal blood perfusion with optical microangiography", *J Biomed Opt.* 15, 026011 (2010).
[10]. Ruikang K. Wang, Lin An, Spencer Saunders, and David J. Wilson, "Optical microangiography provides depth-resolved images of directional ocular blood perfusion in posterior eye segment", *J Biomed Opt.* 15, 020502 (2010).
[11]. Yuankai K. Tao, Kristen M. Kennedy, and Joseph A. Izatt, " Velocity-resolved 3D retinal microvessel imaging using single-pass flow imaging spectral domain optical coherence tomography", *Opt Express*. 17, pp. 4177-4188 (2009) .
[12]. M. Szkulmowski, A. Szkulmowska, T. Bajraszewski, A. Kowalczyk, and M. Wojtkowski, "Flow velocity estimation using joint spectral and time domain optical coherence tomography," *Opt Express*. 16, 6008-6025 (2008).
[13]. Ireneusz Grulkowski, Iwona Gorczynska, Maciej Szkulmowski, Daniel Szlag, Anna Szkulmowska, Rainer A. Leitgeb, Andrzej Kowalczyk, and Maciej Wojtkowski, "Scanning protocols dedicated to smart velocity ranging in Spectral OCT," *Opt Express*. 17, 23736 (2009).
[14]. Lingfeng Yu and Zhongping Chen, "Doppler variance imaging for three-dimensional retina and choroid angiography", *J. Biomed. Opt.*, 15, 016029 (2010).
[15]. David H. Evans, W. Norman McDicken, "Doppler Ultrasound: Physics, Instrumental, and Clinical Applications," 2nd Edition , John Wiley Sons, 2000.
[16]. Hongwu Ren, Kjell Morten Brecke, Zhihua Ding, Yonghua Zhao, J. Stuart Nelson, and Zhongping Chen, "Imaging and quantifying transverse flow velocity with the Doppler bandwidth in a phase-resolved functional optical coherence tomography," *Opt Lett.* 15, 409-411 (2002).
[17]. C. Kasai, K. Namekawa, A. Koyano, R. Omoto, "Real-Time Two-Dimensional Blood Flow Imaging Using an Autocorrelation Technique," *IEEE Trans. Sonics Ultrason*, SU-32, 458-464(1985).
[18]. Arnold P.G. Hoeks, Peter J. Brands, Theo G.J. Arts and Robert S. Reneman, "Subsample volume processing of doppler ultrasound signals," *Ultrasound Med. Biol.* 20, 953-965(1994) .
[19]. V.X.D.Yang, M.L.Gordon, A.Mok, Y.Zhao, Z.Chen, R.S.C.Cobbold, B.C.Wilson, and I.A.Vitkin, "Improved phase-resolved optical Doppler tomography using the Kasai velocity estimator and histogram segmentation," *Opt. Commun.* 208, 209-214 (2002).
[20]. Yang V, Gordon M, Qi B, Pekar J, Lo S, Seng-Yue E, Mok A, Wilson B, Vitkin I., "High speed, wide velocity dynamic range Doppler optical coherence tomography (Part I): System design, signal processing, and performance," *Opt Express*. 11,794-809 (2003).
[21]. Bin Rao, Lingfeng Yu, Huihua Kenny Chiang, Leandro C. Zacharias,Ronald M. Kurtz, Baruch D. Kuppermann, and Zhongping Chen, "Imaging pulsatile retinal blood flow in human eye", *J. Biomed. Opt.* **13**, 040505(2008).
[22]. Shuichi Makita, Youngjoo Hong, Masahiro Yamanari, Toyohiko Yatagai, and Yoshiaki Yasuno, "Optical coherence angiography", *Opt Express*. 14, 7821(2006).
[23]. D avid W. Scott, "Averaged Shifted Histograms: Effective Nonparametric Density Estimators in Several Dimensions," *Ann. Statist.* ,13, 1024-1040(1985).

[24]. Hiroshi Ishikawa, Daniel M. Stein, Gadi Wollstein, Siobahn Beaton, James G. Fujimoto, and Joel S. Schuman, ¨Macular Segmentation with Optical Coherence Tomography," *Investigative Ophthalmology and Visual Science*. 46, 2012-2017(2005).
[25]. Delia Cabrera Fernández, Harry M. Salinas, and Carmen A. Puliafito, "Automated detection of retinal layer structures on optical coherence tomography images," *Opt. Express* 13, 10200-10216 (2005).
[26]. Tapio Fabritius, Shuichi Makita, Masahiro Miura, Risto Myllylä, and Yoshiaki Yasuno, "Automated segmentation of the macula by optical coherence tomography," *Opt Express*. 17, 15659-15669 (2009).